

Prediction of temperature distribution in hardening silica fume-blended concrete

Wang Xiao-Yong*

*Department of Architectural Engineering, College of Engineering, Kangwon National University,
Chuncheon, 200-701, Korea*

(Received May 4, 2013, Revised August 16, 2013, Accepted August 31, 2013)

Abstract. Silica fume is a by-product of induction arc furnaces and has long been used as a mineral admixture to produce high-strength, high-performance concrete. Due to the pozzolanic reaction between calcium hydroxide and silica fume, compared with that of Portland cement, the hydration of concrete containing silica fume is much more complex. In this paper, by considering the production of calcium hydroxide in cement hydration and its consumption in the pozzolanic reaction, a numerical model is proposed to simulate the hydration of concrete containing silica fume. The heat evolution rate of silica fume concrete is determined from the contribution of cement hydration and the pozzolanic reaction. Furthermore, the temperature distribution and temperature history in hardening blended concrete are evaluated based on the degree of hydration of the cement and the mineral admixtures. The proposed model is verified through experimental data on concrete with different water-to-cement ratios and mineral admixture substitution ratios.

Keywords: cement; silica fume; hydration; temperature history; model

1. Introduction

Silica fume (SF) is a by-product of induction arc furnaces in the silicon metal and ferrosilicon alloy industries. SF is a highly pozzolanic cement replacement material because it essentially consists of silica in noncrystalline form with a high specific surface area. The material is mainly used to improve the workability and durability of concrete. In addition, with a view to saving energy and conserving resources, both ecological and economic benefits can be achieved by using SF blended Portland cement (Tang 2010).

As cement hydrates, it generates heat, initially at a rate greater than the heat loss to the environment, and this causes an increase in the temperature of concrete. The continuously casting of concrete may result in the propagation of thermal cracking within structures. The ability to predict the temperature history of concrete would thus be useful to structural engineers and designers interested in producing durable concrete structures. Wang and Dilger (1994) have attempted to predict the temperature rise that occurs in hardening concrete, but the focus of these models has been on following the relationships between the hydration heat rate and concrete

*Corresponding author, Professor, E-mail: wxbrave@kangwon.ac.kr

maturity function under adiabatic conditions. The models have not taken into account the effect of the water-cement ratio (w/c) on hydration heat release. Park *et al.* (2008) built a micro-structural hydration model of Portland cement that considers the reduction in the hydration rate that occurs due to the reduction in the amount of free water and the reduction in the interfacial area of contact between the free water and the hydration products. Chen and An (2012) proposed a hydration model to consider the effects of the particle size distribution of cement and the water-to-cement ratio. The isothermal heat generated by the hydration of cement was evaluated using the proposed model. Tian *et al.* (2013) predicted the heat released and temperature history of hardening concrete using the hydration degree obtained from each time sub-step. Furthermore, based on the equivalent age method, a maturity model was applied to describe the evolution of the mechanical properties of the material during the hydration process.

Compared with that of Portland cement, the hydration of cement incorporating supplementary cementing materials (SCM), such as fly ash, slag or silica fume, is much more complex due to the coexistence of cement hydration and the reactions of the mineral admixtures. Based on the experimental results of reaction stoichiometries among supplementary cementing materials (SCM), chemically bound water and calcium hydroxide, Papadakis (1999, 2000) proposed a chemical-based steady-state model for the supplementary cementing materials of blended cement, which was able to estimate the final material properties, such as porosity and chemically bound water and calcium hydroxide contents. In contrast to Papadakis's chemical-based steady-state model (1999, 2000), kinetic models were proposed to evaluate the development of the properties of blended concrete. De Schutter and Taerwe (1995) proposed a kinetic hydration model valid both for Portland cement and blast furnace slag cement in which the heat evolution of blast furnace slag cement was obtained through the superposition of the heat produced by the Portland reaction and a slag reaction. Han and Kim (2003) proposed a model using apparent activation energy to estimate the variation in the compressive strength of fly ash concrete with aging. It was observed that apparent activation energy was correlated with the fly ash replacement content and water–binder ratio. Based on a multi-component hydration heat model and micro pore structure formation model, Song and Kwon (2009) evaluated chloride penetration in silica fume, fly ash and slag blended concrete using the diffusion coefficients obtained from a neural network algorithm. Maekawa *et al.* (2009) proposed a general hydration model incorporating silica fume, fly ash and slag, whose reactions were treated separately from those of ordinary Portland cement, with some of the interactions being taken into account in terms of the free water content and the calcium hydroxide concentration.

As demonstrated in Papadakis (1999, 2000), De Schutter and Taerwe (1995), Han and Kim (2003), Song and Kwon (2009) and Maekawa *et al.* (2009), it is typical to consider the hydration reactions of cement and blended mineral admixtures to model the hydration of blended concrete. In this paper, a numerical procedure is proposed to simulate the hydration of concrete containing silica fume. The numerical procedure includes two sub-components, a cement hydration model and a silica fume reaction model. The heat evolution rate of silica fume-blended concrete is determined by considering the contributions of cement hydration and the reaction of silica fume. Furthermore, by combining the proposed hydration model with a finite element method, the temperature distribution in the hardening silica fume-blended cement is evaluated. The novelty of this paper lies in the fact that in the proposed hydration model, the heat evolution rate of each element in hardening concrete is dependent on the current node temperature. In other words, the proposed model considers the difference in heat evolution rate between the surface and center of hardening concrete.

2. Hydration model of portland cement

2.1 Modeling of cement hydration

The shrinking-core model, which was originally developed by Tomosawa (1997), is used in this study to simulate the development of cement hydration. This model is expressed as a single equation consisting of three coefficients: k_d , the reaction coefficient in the induction period; D_e , the effective diffusion coefficient of water through the C–S–H gel; and k_r , the coefficient of the reaction rate of cement, as shown in Eq. (1). These coefficients determine the rate of mass transport through the initial shell layer, the rate of the phase boundary reaction and the rate of the diffusion-controlled process. The modeled cement particles are assumed to be spheres surrounded by hydration products. Based on this theory, the rate of cement hydration is derived as shown in Eq. (1).

$$\frac{d\alpha}{dt} = \frac{3(S_w/S_0)\rho_w C_{w-free}}{(v+w_g)r_0\rho_c} \frac{1}{\left(\frac{1}{k_d} - \frac{r_0}{D_e}\right) + \frac{r_0}{D_e}(1-\alpha)^{-\frac{1}{3}} + \frac{1}{k_r}(1-\alpha)^{-\frac{2}{3}}} \quad (1)$$

where α is the degree of cement hydration; v is the stoichiometric ratio by mass of water to cement (= 0.25); w_g (g/g) is the amount of physically bound water in the C–S–H gel (= 0.15); ρ_w (g/cm³) is the density of water; C_{w-free} is the amount of water on the exterior of the C–S–H gel; and r_0 (cm) is the radius of unhydrated cement particles.

In Eq. (1), the cement particles are assumed to be spherical and of uniform size with an average radius of $r_0 = 3/(S\rho_c)$ (Tomosawa 1997). The terms S and ρ_c (g/cm³) represent the Blaine surface area and density of the cement, respectively. As hydration progresses, the hydration rate decreases with the decrease in the contact area between cement particles and the surrounding water because of the increase in the number of contact points among cement particles. This effect is accounted for by the term (S_w/S_0) in Eq. (1), where S_w is the effective surface area of the cement particles in contact with water and S_0 is the total surface area if the surface area develops in an unconstrained manner (Tomosawa 1997).

The reaction coefficient k_d (cm/h) is assumed to be a function of the degree of hydration as shown in Eq. (2), where B (cm/h) and C (cm/h) are the coefficients determining this factor

$$k_d = \frac{B}{\alpha^{1.5}} + C\alpha^3 \quad (2)$$

In Tomosawa (1997) and Park *et al.* (2008), the effective diffusion coefficient D_e was assumed to be affected by the tortuosity and pore size of the C–S–H gel and was expressed using a term describing the degree of hydration as shown in Eq. (3). If the C–S–H gel is very porous and the pore network shows low tortuosity, the value of D_e (cm²/h) will be high and ions will easily

diffuse through the gel. D_{e0} (cm²/h) is the initial effective diffusion coefficient of water when the C–S–H gel is still only loosely formed during the early period after mixing. With the progress of hydration, the thickness of the C–S–H layer increases, and the diffusivity of water through this layer decreases. In Tomosawa (1997) and Park *et al.* (2008), this effect was expressed by the term $\ln(1/\alpha)$, as shown in Eq. (3)

$$D_e = D_{e0} \ln\left(\frac{1}{\alpha}\right) \quad (3)$$

The physical meanings of the parameters in the hydration model are summarized as follows

B is the coefficient of formation of the initial impermeable layer, C is the coefficient of destruction of the initial impermeable layer, k_r is the chemical reaction rate coefficient and D_{e0} is the initial diffusion coefficient.

In addition, free water in the capillary pores is depleted as the hydration of cement minerals progresses. Some water is bound in the gel pores, and this water is not available for further hydration, an effect that must be taken into consideration in every step of the hydration process. Therefore, the amount of water in the capillary pores C_{w-free} is expressed as a function of the degree of hydration in the previous step, as shown in Eq. (4).

$$C_{w-free} = \frac{W_0 - 0.4 * \alpha * C_0}{W_0} \quad (4)$$

where C_0 (kg/m³) and W_0 (kg/m³) are the mass fractions of cement and water in the mix proportion, respectively.

The effect of temperature on these reaction coefficients is assumed to follow Arrhenius's law, as shown in Eqs. 5(a)–(d) (Tomosawa 1997)

$$B = B_{20} \exp\left(-\beta_1 \left(\frac{1}{T} - \frac{1}{293}\right)\right) \quad (5a)$$

$$C = C_{20} \exp\left(-\beta_2 \left(\frac{1}{T} - \frac{1}{293}\right)\right) \quad (5b)$$

$$D_e = D_{e20} \exp\left(-\beta_3 \left(\frac{1}{T} - \frac{1}{293}\right)\right) \quad (5c)$$

$$k_r = k_{r20} \exp\left(-\frac{E}{R} \left(\frac{1}{T} - \frac{1}{293}\right)\right) \quad (5d)$$

where β_1 (K), β_2 (K), E/R (K) and β_3 (K) are temperature sensitivity coefficients and B_{20} , C_{20} , k_{r20} and D_{e20} are the values of B , C , k_r and D_e , respectively, at 20°C. The values of the temperature sensitivity coefficients can be calibrated by using experimental results regarding the degree of hydration at different curing temperatures.

The rate of heat evolution of the hydrating cement is proportional to the hydration reaction rate,

as shown in Eq. (6)

$$\frac{dQ}{dt} = C_0 * \sum g_i H_i \frac{d\alpha}{dt} \quad (6)$$

where $\frac{dQ}{dt}$ is the rate of heat evolution, g_i is the weight fraction of the individual components of the cement and H_i (kJ/kg) is the total heat generation of the individual components of the cement (Tomosawa 1997 and Park *et al.* 2008).

Based on the hydration model, the incremental temperature increase of hardening concrete in one time step under adiabatic conditions can be calculated as follows

$$\Delta T = \frac{dQ(t)}{Cp(t)} \quad (7)$$

where ΔT is the incremental temperature change in one time step; $dQ(t)$ is the released heat calculated using Eq. (6); and $Cp(t)$ is the heat capacity of the hardening concrete, which can be calculated as the sum of the individual components of the concrete (the heat capacities of cement, sand, aggregate, water and chemically bound water are 0.84 J/g°C, 0.9 J/g°C, 0.9 J/g°C, 4.18J/g°C and 2.2 J/g°C, respectively) (Tomosawa 1997 and Park *et al.* 2008). It should be noted that in the proposed model, the heat capacity of chemically bound water (2.2 J/g°C) is lower than that of water (4.18J/g°C). As hydration proceeds, the overall heat capacity of the concrete mixture decreases by approximately 5% as free water is bound by the hydration products, in relatively good agreement with the experimental results of De Schutter and Taerwe (1995).

2.2 Parameter study of portland cement hydration model

In Tomosawa's original hydration model (1997) and the improved model developed by Park *et al.* (2008), the hydration reaction coefficients B , C , D_e and k_r were obtained by fitting the experimental results obtained for the rate of heat evolution of hydrating cement paste. When the mineral composition of the cement or water-to-cement ratio varied, a new regression was necessary to obtain the values of the hydration reaction coefficients. By contrast, in the multi-component hydration model of Maekawa *et al.* (2009), the hydration reactions of the mineral constituents of cement, such as the hydration reactions of C_3S , C_2S , C_3A and C_4AF , are separated from each other. The evolution of the hydration of cement with different mineral compositions can be automatically calculated without any regressions.

The hydration of cement is a highly nonlinear process involving complex interactions. In this section, Maekawa *et al.*'s experimental results (2009), including the early-stage temperature rise and the evolution of chemically bound water, are adopted to calibrate and verify the proposed model. The specimens submitted to an adiabatic temperature test are composed of concrete, and the specimens submitted to a chemically bound water test are composed of cement paste. In the regression, five types of Portland cement were tested, i.e., ordinary Portland cement (OPC), early-hardening cement (HPC), moderate-heat cement (MPC), low-heat cement (LPC) and belite-rich cement (BRC). The effects of casting temperature, water-to-binder ratio and mineral compositions

on hydration are investigated by carrying out an experimental program with conditions analogous to those observed at construction sites. As described previously, the effects of a low water-to-cement ratio on the heat of hydration generation were considered in this study. For an adiabatic temperature test employing a unit cement weight of 400 kg, the water-to-cement ratio is approximately 40%. It is well known that at least 40% cement weight of water is required for the complete hydration of Portland cement. For the chemically combined water test, a lower water-to-cement ratio of 0.3 is used, which enhances the sensitivities of the hydration reactions to the amounts of available water.

Based on the test results regarding the rise in adiabatic temperature (Maekawa *et al.* 2009), we calibrated the hydration reaction coefficients of the hydration model. The mineral compositions of the five types of Portland cement considered are shown in Table 1. The C_3S contents varied from 5.2% (BRC) to 64.2% (HPC), the C_2S contents varied from 11.8% (HPC) to 74.7 (BRC) and the C_3A contents varied from 1.7% (BRC) to 10.4% (OPC). The concrete mix proportions are shown in Table 2. Three unit cement weights were examined for each type of cement. The water-to-cement ratios of the specimens varied between 0.4 and 0.785. In the experiments on the rise in adiabatic temperature, three casting temperatures (10°C, 20°C and 30°C) were examined. In the case of OPC concrete and MPC concrete, a delay-type AE water-reducing agent was used. For other mix proportions, the water-reducing agent was not a delay-type additive.

For each type of cement, nine adiabatic temperature rise tests were carried out (three unit cement weights performed for three different casting temperatures). Based on the experimental results obtained for the rise in the adiabatic temperature of hardening concrete, we can calibrate the hydration reaction coefficients of each type of cement by using a predictor-corrector algorithm. Because the effects of the water-to-cement ratio, Blaine surface area of cement and curing temperature on the hydration reaction have been considered in the proposed hydration model, the calibrated hydration reaction coefficients are independent of the water-to-cement ratio, Blaine surface area and curing temperature and depend only on the mineral compositions of Portland cement. Furthermore, we can derive the equations relating the hydration reaction coefficients to cement mineral compositions

$$B_{20} = 6 * 10^{-12} * (C_3S\% + C_3A\%) + 4 * 10^{-10} \quad (8a)$$

$$C_{20} = 0.0003 * C_3S\% + 0.0186 \quad (8b)$$

$$kr_{20} = 8 * 10^{-8} * C_3S\% + 1 * 10^{-6} \quad (8c)$$

$$De_{20} = -8 * 10^{-12} * C_2S\% + 7 * 10^{-10} \quad (8d)$$

$$\beta_1 = 1000 \quad (8e)$$

$$\beta_2 = 1000 \quad (8f)$$

$$E/R = 5400 \quad (8g)$$

$$\beta_3 = 7500 \quad (8h)$$

Table 1 Mineral compositions of portland cement.

	Mineral composition (mass %)					Blaine(cm ² /g)
	C ₃ S	C ₂ S	C ₃ A	C ₄ AF	$\overline{CS_2H}$	
OPC	47.2	27.0	10.4	9.4	3.9	3380
HPC	64.2	11.8	9.2	8.9	6.45	4210
MPC	44.4	33.7	3.7	12.5	3.9	3040
LPC	25.0	55.0	3.0	9.0	5.59	3390
BRC	5.2	74.7	1.7	12.2	4.09	2970

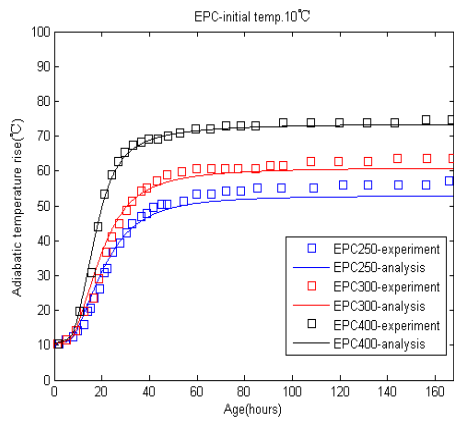
Table 2 Mix proportions of portland cement concrete.

	Water (kg/m ³)	Cement (kg/m ³)	Sand (kg/m ³)	Aggregate (kg/m ³)	Water-to- binder ratio	Water reducing agent (Cement×%)
OPC400	157	400	658	1129	0.392	0.25*
OPC300	148	300	765	1129	0.493	0.25*
OPC200	157	200	862	1089	0.785	0.25*
HPC400	152	400	730	1129	0.38	0.25
HPC300	143	300	813	1129	0.477	0.25
HPC250	143	250	869	1089	0.572	0.25
MPC400	157	400	663	1129	0.392	0.25*
MPC300	148	300	770	1129	0.493	0.25*
MPC200	157	200	865	1089	0.785	0.25*
LPC260	145	260	844	1082	0.558	0.25
LPC300	145	300	811	1082	0.483	0.25
LPC340	145	340	779	1082	0.426	0.25
BRC	168	305	750	1089	0.551	0.25

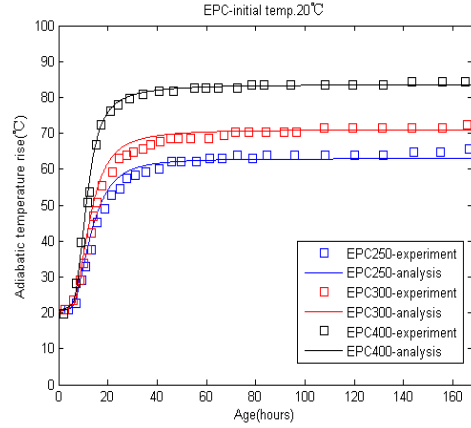
*delay-type additive

As shown in Eq. 8(a), Eq. 8(b) and Eq. 8(c), with the increase in the C₃S and C₃A contents, the values of the hydration rate coefficients B_{20} , C_{20} and k_{r20} will increase, which indicates that cement with higher C₃S and C₃A contents will exhibit a higher hydration speed. In addition, as shown in Eq. 8-d, the hydration rate coefficient D_{e20} decreases with the increase in the C₂S content. This result suggests that cement with a higher C₂S content, such as low-heat Portland cement and belite-rich cement, will exhibit a lower reactivity than other types of cement. On the other hand, based on the investigation of the degree of hydration of Portland cement with different mineral compositions, Park *et al.* (2008) and Maruyama *et al.* (2005) observed that the temperature sensitivity coefficients β_1 , β_2 , E/R and β_3 can be approximated as constants for each type of cement. Therefore, by fitting the experimental results regarding the rise in adiabatic temperature using Eqs. 8-e to 8-h, the values of β_1 , β_2 , E/R and β_3 are determined to be 1000, 1000, 5400 and 7500, respectively.

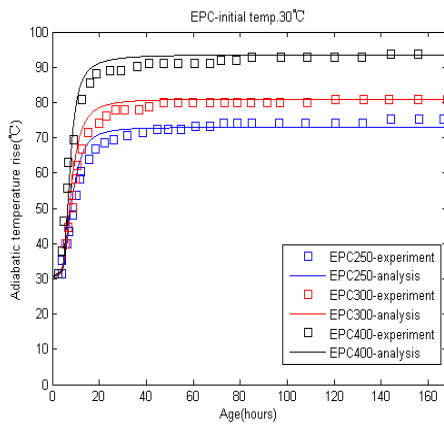
Fig. 1 compares the experimental and calculated results obtained by using Eqs. 8-a to 8-h. As shown in this figure, the prediction results generally agree with the experimental results. The decrease in the rise in adiabatic temperature upon the completion of the reaction when the water-



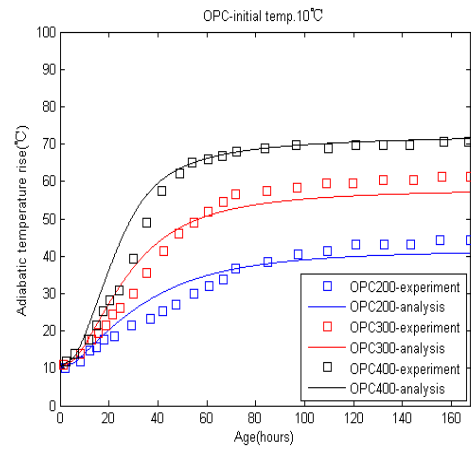
(a) EPC- initial temperature 10°C



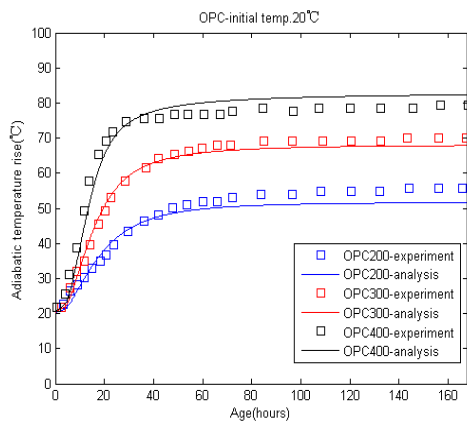
(b) EPC- initial temperature 20°C



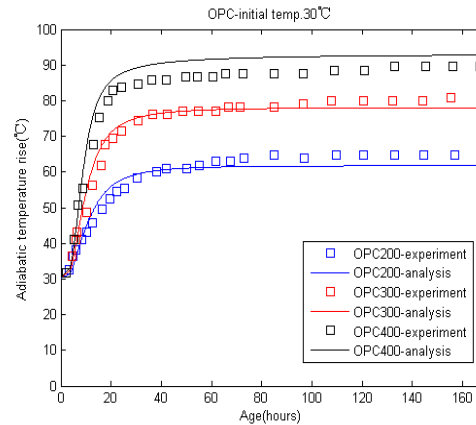
(c) MPC- initial temperature 10°C



(d) MPC- initial temperature 20°C

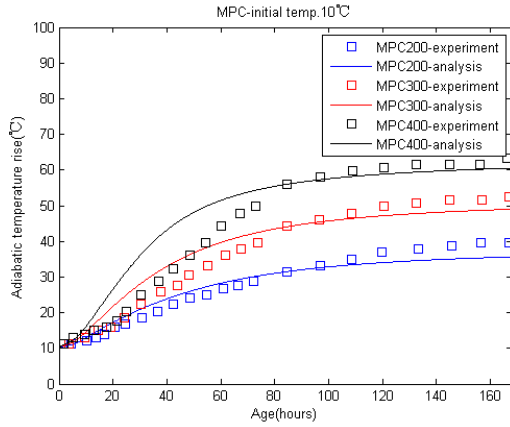


(e) OPC- initial temperature 20°C

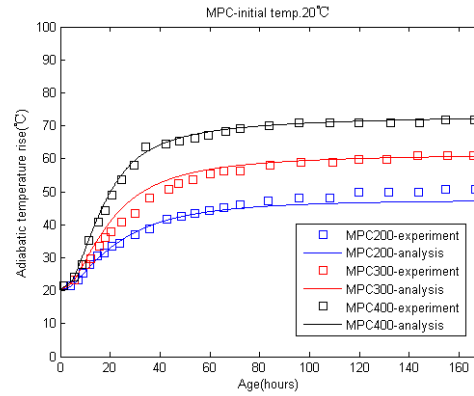


(f) OPC- initial temperature 30°C

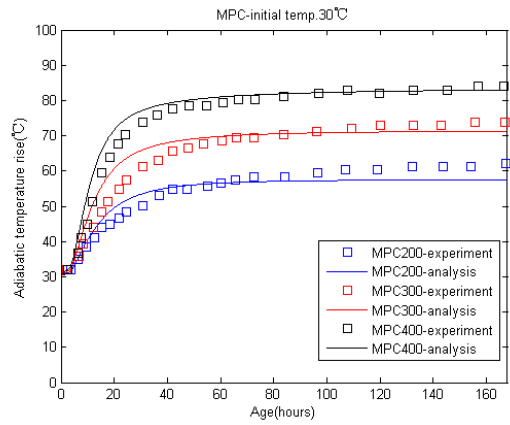
Fig. 1 The comparison between experimental results and prediction results of adiabatic temperature rise of Portland cement concrete



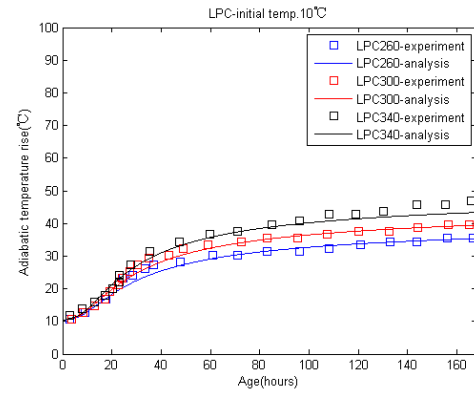
(g) MPC- initial temperature 10°C



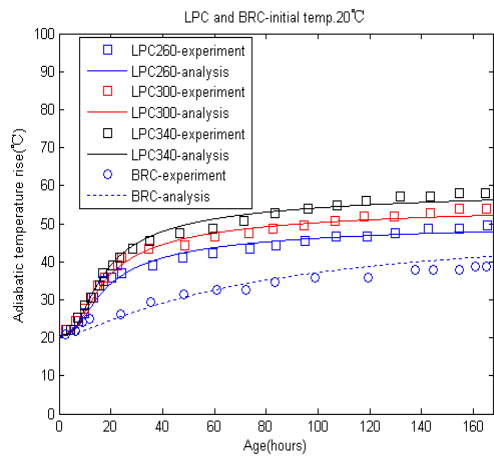
(h) MPC- initial temperature 20°C



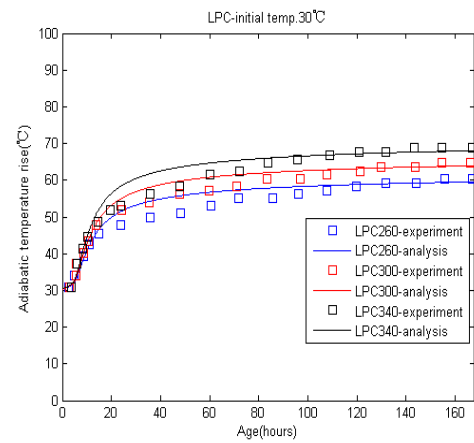
(i) MPC- initial temperature 30°C



(j) LPC- initial temperature 10°C

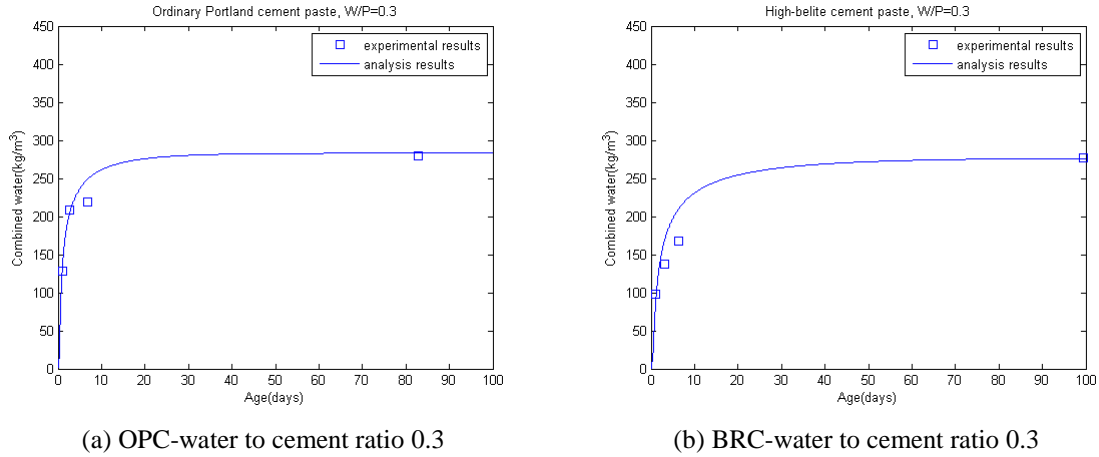


(k) LPC and BRC- initial temperature 20°C



(l) LPC - initial temperature 30°C

Fig. 1 Continued



(a) OPC-water to cement ratio 0.3

(b) BRC-water to cement ratio 0.3

Fig. 2 The comparison between experimental results and prediction results of chemically bound water of Portland cement paste

to-cement ratio is low was accurately modeled. However, for some cases, such as those of the OPC concrete with an initial temperature of 10°C (Fig. 1-d), MPC concrete with a casting temperature of 10°C (Fig. 1(g)) and LPC concrete with different casting temperatures (Fig. 1(j), Figs. 1(k) and (l)), the predicted results are slightly different from the experimental results. This discrepancy is because some factors were neglected in the simulation.

As shown in Fig. 1(d) (OPC concrete with a casting temperature of 10°C) and Fig. 1(g) (MPC concrete with a casting temperature of 10°C), at an early age of 2 days, the analysis results are slightly higher than the experimental results. This difference may be due to the neglect of the delay effect of delay-type additives in the simulation (for OPC and MPC concrete, a delay-type AE water-reducing agent is used, whereas for EPC and LPC, the adopted AE water-reducing agent is not a delay-type agent). When the casting temperature was lower (10°C), the hydration rate of cement becomes much slower, and the delay effect of delay-type additives on cement hydration becomes much more significant. By contrast, when considering the delay effect of delay-type additives, the model of Maekawa *et al.* (2009) shows better prediction results than my model.

On the other hand, Maekawa *et al.* (2009) proposed that the mineral compositions of cement, such as C_3S , C_2S , C_3A and C_4AF , show different thermal activities. The order of mineral thermal activity is $C_3A > C_3S > C_4AF > C_2S$. Therefore, cements with different mineral compositions may present different temperature sensitivity coefficients. Compared with OPC, LPC has a relatively higher C_2S content. Hence, the actual temperature sensitivity coefficients of LPC may be lower than the proposed values (Eqs. 8(e) to 8(h)). For LPC concrete, ignoring this difference regarding the temperature sensitivity coefficients make the analysis results higher than the experimental results (Fig. 1(l), LPC concrete with a casting temperature of 30°C).

In addition, Maekawa *et al.* (2009) reported that the reactivity of C_3S is much higher than that of C_2S , and a stagnated C_2S particle can act as a precipitation site for hydration products from C_3S , which is known as the micro-filler effect. Compared with OPC, LPC presents a higher C_2S content. Thus, the micro-filler effect will be significant for LPC concrete. To accurately model the micro-filler effect, the difference in reactivity between C_3S and C_2S should be modeled. Neglecting the micro-filler effect will make the analysis results lower than the experimental

results. By contrast, due to the concise consideration of various factors, the model of Maekawa *et al.* (2009) yields better prediction results regarding temperature rises in LPC concrete than my model.

The aforementioned factors simultaneously affect the hydration of LPC concrete to different extents. Depending on these variables, the model predicts the measured values with different degrees of accuracy (Fig. 1(j), Fig. 1(k) and (l)).

Summarily, the proposed model is currently limited in that some variables are not accounted for. This model will be the subject of further improvement in the future.

By using the hydration reaction coefficients shown in Eqs. (8(a) to 8(h)), the degree of hydration of Portland cement can be calculated as a function of curing age. Furthermore, the chemically bound water of hardening concrete can be determined from the degree of hydration of cement. In a series of experiments on chemically combined water (Maekawa *et al.* 2009), the water-to-cement ratio of the specimens by weight was determined to be 0.3, which is typical of a powder-rich high-performance concrete used in construction sites. When experiments on chemically bound water were performed, the specimens were sealed and cured at a constant temperature of 20°C. The amounts of chemically bound water were measured by performing differential thermogravimetric analysis (TGA). Fig. 2 compares the experimental and predicted results for chemically bound water. The predicted results generally agree with the experimental results. It can be observed that a substantial increase in the amount of bound water occurs after several weeks in the case of belite-rich cement paste (Fig. 2(b)), whereas for OPC paste, the reactions essentially stop after approximately four weeks under sealed conditions (Fig. 2(a)).

3. Hydration model for cement blended with silica fume

3.1 Amount of calcium hydroxide (CH) during the hydration process

Maekawa *et al.* (2009) performed a systematic investigation of the hydration, microstructural formation and mass transport of Portland cement concrete and blended concrete. Based on an analysis of the experimental results regarding the amount of chemically bound water, increase in adiabatic temperature and measured temperature of small quasi-adiabatic blocks, Maekawa stated that the reaction of silica fume can be roughly described by the following approximate key figures:

Calcium hydroxide	2.00 g/g silica fume
Chemically bound water	0 g/g silica fume (Lura <i>et al.</i> 2003)
Gel water	0.5 g/g silica fume (Lura <i>et al.</i> 2003)
Total heat generation	565 kJ/kg silica fume

Using the hydration model and the stoichiometry of the reaction of silica fume proposed by Maekawa *et al.* (2009), the amounts of calcium hydroxide, chemically bound water and capillary water in cement-silica fume blends during hydration can be determined using the following equations

$$CH = RCH_{CE} * C_0 * \alpha - RCH_{SF} * \alpha_{SF} * P \quad (9)$$

$$W_{cap} = W_0 - 0.4 * C_0 * \alpha - RCW_{SF} * \alpha_{SF} * P - RPW_{SF} * \alpha_{SF} * P$$

(10)

$$W_{cbm} = v * C_0 * \alpha + RCW_{SF} * \alpha_{SF} * P$$

(11) In Eqs. (9), (10) and (11), CH , W_{cap} and W_{cbm} are the masses of calcium hydroxide, capillary water and chemically bound water, respectively; α_{SF} is the ratio between the released heat and the total heat generation of the silica fume; P is the mass of the silica fume in the mixture proportion; RCH_{CE} is the mass of calcium hydroxide produced from the hydration of cement; RCH_{SF} is the mass of reacted calcium hydroxide in the reaction of silica fume; RCW_{SF} is the mass of chemically bound water in the reaction of silica fume; and RPW_{SF} is the mass of gel water in the reaction of silica fume. As shown in Eq. (9), the evolution of the mass of calcium hydroxide depends on two factors: the production of calcium hydroxide from the hydration of Portland cement and its consumption due to the chemical activity of the mineral admixtures. As shown in Eq. (10), capillary water is consumed by both cement hydration and the reaction of the mineral admixtures. As shown in Eq. (11), both the hydration of Portland cement and the reaction of mineral admixtures contribute to the formation of chemically bound water.

3.2 Simulation of the pozzolanic reaction in cement-silica fume blends

SF belongs to the category of highly pozzolanic materials because it essentially consists of silica in non-crystalline form with a high specific surface area and thus exhibits great pozzolanic activity (reaction with calcium hydroxide). Based on the experimental research of heat evolution of silica fume-blended cement, Papadakis (1999 and 2000) proposed that pozzolanic activity is a diffusion-controlled process. Hyun (1995) proposed that the kinetic reaction of mineral admixtures is similar to that of cement and that the hydration rate of pozzolanic materials depends on the amount of calcium hydroxide in hydrating blends and the degree of hydration of the mineral admixtures. Due to the high specific surface area and great pozzolanic activity of SF, in the present paper, it is assumed that the hydration of SF involves two processes: a phase-boundary reaction process and a diffusion process. Thus, based on the method proposed by Saeki and Monteiro (2005), the hydration equation of silica fume can be written as follows

$$\frac{d\alpha_{SF}}{dt} = \frac{m_{CH}(t)}{P} \frac{3\rho_w}{v_{SF} r_{SF0} \rho_{SF}} \frac{1}{\frac{r_{SF0}}{D_{eSF}} (1-\alpha_{SF})^{\frac{-1}{3}} - \frac{r_{SF0}}{D_{eSF}} + \frac{1}{k_{rSF}} (1-\alpha_{SF})^{\frac{-2}{3}}} \quad (12-1)$$

$$D_{eSF} = D_{eSF0} * \ln\left(\frac{1}{\alpha_{SF}}\right) \quad (12-2)$$

where $m_{CH}(t)$ (kg/m^3) is the mass of calcium hydroxide in a unit volume of hydrating cement-silica fume blends, which can be obtained from Eq. (9); P (kg/m^3) is the silica fume mass in the mixing proportion; v_{SF} is the stoichiometric ratio of the mass of CH to silica fume; r_{SF0} ($=0.18 \mu\text{m}$) is the radius of a silica fume particle; ρ_{SF} (g/cm^3) is the density of the silica fume; D_{eSF0} (cm^2/h) is the initial diffusion coefficient; and k_{rSF} (cm/h) is the reaction rate coefficient.

The effect of temperature on the silica fume reaction is considered to follow the Arrhenius law as follows

$$D_{eSF0} = D_{eSF20} \exp(-\beta_{3SF} (\frac{1}{T} - \frac{1}{293})) \quad (12-3)$$

$$k_{rSF} = k_{rSF20} \exp(-\frac{E_{SF}}{R} (\frac{1}{T} - \frac{1}{293})) \quad (12-4)$$

where D_{eSF20} and k_{rSF20} are the values of D_{eSF} and k_{rSF} at 293 K, respectively, and β_{3SF} (K) and E_{SF}/R (K) are the temperature sensitivity coefficients of D_{eSF} and k_{rSF} , respectively.

The released heat of the hydrating blends is the result of the heat released from Portland cement hydration and the heat released from the mineral admixture reaction. The total released heat is expressed by Eq. (13)

$$\frac{dQ}{dt} = C_0 * \sum g_i H_i \frac{d\alpha}{dt} + P * H_{SF} * \frac{d\alpha_{SF}}{dt} \quad (13)$$

where the first term derives from the hydration of Portland cement and the second derives from the reaction of silica fume; H_{SF} is the total heat generation content of the silica fume (by comparing the analytical and experimental data, Maekawa *et al.* (2005) set the total heat generation of silica fume to 565 kJ/kg).

3.3 Prediction of the rise in adiabatic temperature of concrete containing silica fume

Maekawa *et al.* (2009) conducted a series of adiabatic temperature rise tests on concrete containing silica fume in three different ratios (10%, 20% and 30% in the mixtures SF10, SF20 and SF30, respectively) using plain mixtures as the controls (C297, C264 and C231, respectively). The mixing proportions are shown in Table 3. The plain mixture contained the same unit content of Portland cement as the silica fume-blended concrete so that the heat generated by silica fume could be detected by comparing rises in adiabatic temperature.

Based on the experimental results regarding the adiabatic temperature increase of silica fume-blended concrete and the predictor-corrector algorithm, the parameters related to the silica fume reaction can be calibrated. The reaction coefficients of silica fume are calibrated and shown in Table 4. These fit parameters for silica fume do not change from one mix to another. Fig. 3 compares the analysis results and experimental results. The analysis results can generally reproduce the experimental results. As shown in Fig. (3-b), in the case of silica fume-blended concrete, given a certain water-to-binder ratio, the rise in adiabatic temperature will decrease with the increase in the silica fume replacement ratios due to a shortage of calcium hydroxide. On the other hand, for concrete incorporating a higher silica fume content (when the silica fume replacement ratio is 30%), at ages between 1 day and 2 days, the analysis results are slightly lower than the experimental results. This result is observed because of the micro-filler effect of stagnated silica fume particles on the hydration of cement is ignored (when the silica fume replacement ratio is higher, the pozzolanic reaction of silica fume will stagnate due to the shortage of calcium hydroxide, and the stagnated fine silica fume particles will have a micro-filler effect on the reacting cement components).

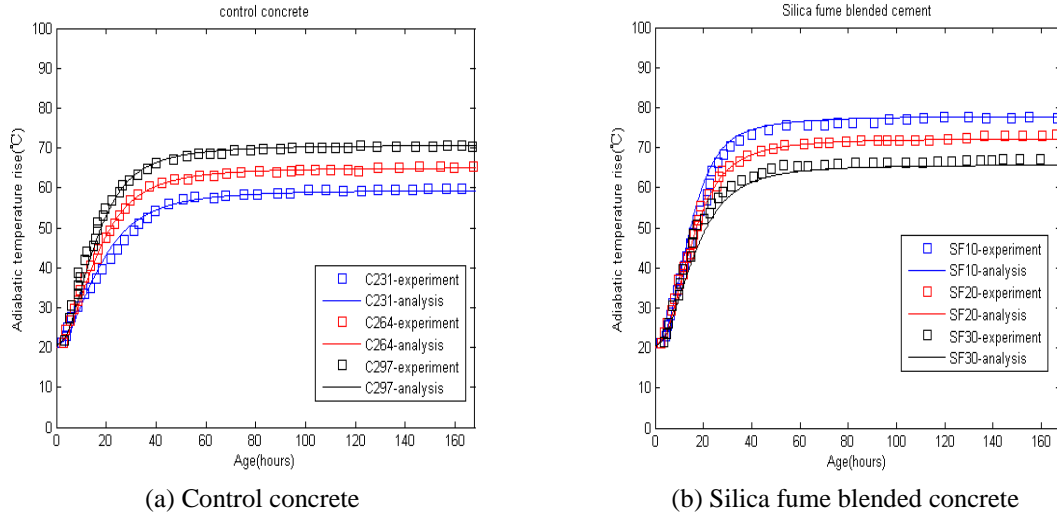


Fig. 3 The comparison between experimental results and prediction results of adiabatic temperature rise of silica fume blended concrete

Table 3 Mixing proportions of concrete containing silica fume with their control mixtures

	Water to binder ratio(%)	Unit weight(kg/m ³)				
		Water	Cement	Silica fume	Sand	Aggregate
SF10	50	165	297	33	792	999
SF20	50	165	264	66	780	999
SF30	50	165	231	99	769	999
C297	55.5	165	297	-	817	1014
C264	62.5	165	264	-	844	1014
C231	71.4	165	231	-	872	1014

Table 4 Coefficients of silica fume reaction model

k_{rSL20} (cm/h)	D_{eSL20} (cm ² /h)	β_{3SL} (K)	$\frac{E_{SL}}{R}$ (K)
1.80×10^{-9}	1.92×10^{-12}	7000	5000

When silica fume is incorporated into concrete, there are two possible reasons why there is a change in the generation of heat. One is the pozzolanic reaction of amorphous silica in SF, and the other is the effect of SF on the heat of cement hydration. In the current paper, a new model that can describe the pozzolanic reaction between calcium hydroxide and SF is proposed. Moreover, the effect of SF on the heat of cement hydration is considered by accounting for the amount of capillary water (Eq. (10)) and the dilution effect (Eq. (4)). Hence, the proposed model shows a strong ability to predict the development of the properties of silica fume concrete, such as the rise in temperature under adiabatic conditions.

4. Description of a temperature prediction model

4.1 Description of a temperature prediction model

4.1.1 The Governing equation of the model

At any time, the temperature distribution in a hardening concrete is represented by a dynamic heat balance between the heat generated inside the concrete and heat lost to the surroundings. The heat generation inside is due to the hydration reactions of the cement and the mineral admixtures. The temperature distribution is determined by the following heat equation (Park *et al.* 2008)

$$\rho C \frac{\partial T}{\partial t} = \text{div}(k \nabla T) + \frac{dQ}{dt} \quad (14)$$

where (ρC) is the heat capacity of hydrating concrete and can be calculated as the sum of the individual components of concrete; k is the thermal conductivity of concrete; T is the concrete temperature; t is time; and $\frac{dQ}{dt}$ is the heat generation rate in hardening concrete, which can be calculated based on the degrees of hydration of the cement and the mineral admixtures (Eq. (13)).

4.1.2 Boundary and initial conditions

Eq. (14) is subject to two types of boundary conditions. The first is that the temperature along the boundary or around a portion of the boundary is known, and the second is that the energy transferred through the boundary is known. For ordinary engineering structures, the second type of boundary condition normally holds. This boundary condition can be described by the following equation (Tomosawa 1997 and Park *et al.* 2008):

$$k \nabla T = \beta (T_s - T_a) \quad (15)$$

where β is the heat convection coefficient between the surface of the concrete and the surrounding environment; T_s is the temperature on the surface of the concrete; and T_a is the temperature of the surrounding environment.

The initial condition can be described by the following equation

$$T|_{t=0} = T_0 \quad (16)$$

where T_0 is the initial temperature of the concrete member.

4.1.3 Numerical method for solving the governing equation

In this paper, a finite element method is adopted to solve Eq. (14). Eight-node isoparametric elements are built to model the volume of concrete in three-dimensional (3D) space. Following the 3D approximation, Eq. (14) can be rewritten as follows (Park *et al.* 2008)

$$[B]\{T\} + [C] \frac{\partial \{T\}}{\partial t} = \{P\} \quad (17)$$

In Eq. (17), the global matrices $[B]$, $[C]$ and $\{P\}$ are obtained from the assembly of the element matrices as follows:

$$[B] = \sum_e [b]_{ij}^e \quad (18-1)$$

$$[C] = \sum_e [b]_{ij}^e \quad (18-2)$$

$$\{P\} = \sum_e [P]_i^e \quad (18-3)$$

Furthermore, based on numerical time integration, Eq. (17) can be written as follows

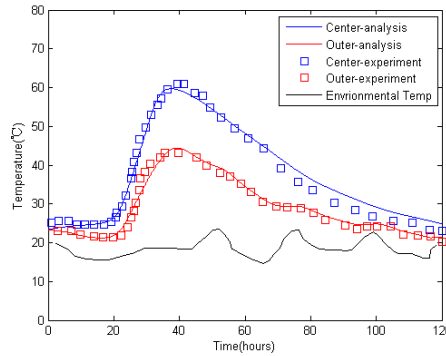
$$\left(\frac{1}{\Delta t}[C] + \theta[B]\right)\{T\}_{n+1} = \left(\frac{1}{\Delta t}[C] - (1-\theta)[B]\right)\{T\}_n + \{P\}_n \quad (19)$$

Generally, the value of parameter θ should be greater than 0.5 to ensure the stability of the numerical integration. In this paper, based on the Galerkin method in the time domain, the value of parameter θ is determined to be 2/3.

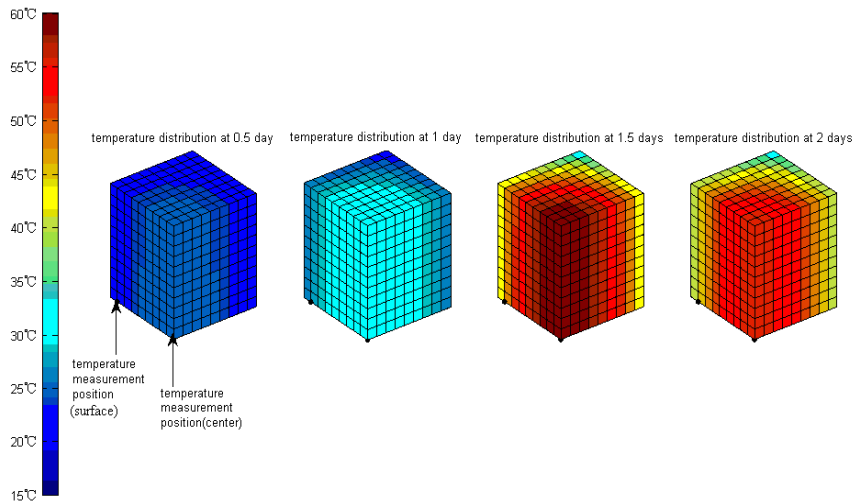
4.2 Prediction of temperature distribution in hardening silica fume-blended concrete

Maruyama *et al.* (2005) conducted an experimental investigation on the temperature distribution in hardening silica fume-blended concrete. Low-heat Portland cement was used, and the water-to-binder ratio and silica fume replacement ratio were 15% and 10.5%, respectively. The dosage of superplasticizer was determined to have a flow value of 60 cm, and the air content was determined to be 2%. A full-scale model column (section 900 mm*900 mm and height 1100 mm) was equipped to measure the temperature history. The specimen was located in an enclosed experiment room. The change in environmental temperature was continuously recorded throughout the entire experiment. Thermocouples were installed at the center and at a point 50 mm from the surface to measure the temperature. The top and bottom surfaces of the specimen were thermally insulated with 100-mm-thick polystyrene foam, and the formworks in the surrounding four faces were metal molds. The thermal conductivity of the concrete was 1.5 W/(m·K), and the heat transfer coefficient between the covered surfaces of the metal molds and the surrounding environment was 10 W/(m²·K) (Maruyama *et al.* 2005).

Finite element modeling with 3D elements was used for the temperature analysis. Because of the symmetry of the geometry, boundary conditions and initial conditions, the FEM mesh and calculation were only applied for one-eighth of the specimens. The boundary conditions of the symmetry planes were treated as insulated boundary conditions ((Park *et al.* 2008). For the analytical discretization of the concrete blocks, 891 (9 × 9 × 11 = 891) eight-node brick elements were used. The dimensions of each element were 50 mm × 50 mm × 50 mm. In the modeling procedure, the concrete column was first divided into discrete elements, and the heat evolution rate of each element in one time step was calculated using a hydration model based on the current element temperature. Fig. (4-a) compares the experimental results and the calculated results. The calculated results generally reproduce the experimental temperature history. The maximum temperature at the center of the specimen reached 60°C from an initial temperature of 23°C. It is noteworthy that the dormant period, which is reflected by the sudden increase in temperature, is quite prolonged. The sudden increase in temperature occurred approximately 24 hours after



(a) Temperature history in hardening silica fume blended concrete



(b) Temperature distribution in hardening silica fume blended concrete

Fig. 4 The temperature history and temperature distribution in hardening silica fume blended concrete

casting, when conventional concrete shows a peak in temperature. This phenomenon can be explained by the addition of the superplasticizer, which has a delay effect on the hydration of cement (in this part of the study, to fit the prolonging of the initial dormant period, the coefficient B_{20} was multiplied by a coefficient of 0.2, whereas the other coefficients were left unchanged.). Fig. (4-b) shows the temperature distribution in concrete specimens 0.5 days, 1 day, 1.5 days and 2 days after casting, illustrating that the maximum temperatures in the block concretes occurred at the centers of the specimens.

The temperature distribution and temperature history in hardening concrete depends on factors such as the heat evolution of hydration, the geometry of the structural members, the initial conditions and the boundary conditions (Wang and Lee 2010). The value of this work lies in the determination of the heat evolution through a hydration model that considers both cement

hydration and the reaction of the mineral admixtures (Park *et al.*'s model (2008) does not consider the reaction of the mineral admixtures.). Mutual interactions between cement hydration and the reaction of the mineral admixtures are considered based on the amount of capillary water and the amount of calcium hydroxide left in the system (De Schutter and Taerwe's model (1995) separates the slag reaction from cement hydration but does not consider the interactions between cement hydration and the reaction of mineral admixtures.). The hydration model is verified through both adiabatic temperature rise tests on concrete with various casting temperatures, water-to-binder ratios and mineral admixture replacement ratios. This model also can be integrated into other commercial software as a module for predicting the properties of hardening blended concrete.

5. Conclusions

In this paper, a numerical model was proposed to simulate the hydration of concrete incorporating silica fume. The numerical model includes two sub-components, a cement hydration model and a silica fume reaction model. First, based on the experimental results of the increase in adiabatic temperature of Portland cement with different mineral compositions, the hydration reaction coefficients in the cement hydration model were calibrated and expressed as functions of the mineral compositions of Portland cement. Second, by considering the production of calcium hydroxide during cement hydration and its consumption in the reactions of silica fume, the reaction of silica fume was separated from that of cement hydration. The heat release rate was determined by considering the contributions of both cement hydration and the reactions of mineral admixtures. Furthermore, three-dimensional finite element thermal analysis was performed to model the transient heat transfer between the concrete and the surroundings as a function of concrete mixture, thermal boundary conditions and environmental conditions. The predicted temperature history curves were compared with experimental data, and a good correlation was observed.

Acknowledgements

This paper is financially supported by National Research Foundation of Korea. (Grant number: NRF-2013R1A1A2060231 ; Project name: An integrated program for predicting chloride penetration into reinforced concrete structures by using a Cement Hydration Model).

References

- Chen, C. and An, X. (2012), "Model for simulating the effects of particle size distribution on the hydration process of cement", *Comput. Concr.*, **9**(3), 179-193.
- De Schutter, G. and Taerwe, L. (1995), "General hydration model for Portland cement and blast furnace slag cement", *Cement Concrete Res.*, **25**(3), 593-604.
- Han, S.H., Kim, J.K. and Park, Y.D. (2003), "Prediction of compressive strength of fly ash concrete by new apparent activation energy function", *Cement Concrete Res.*, **33**(7), 965-971.
- Hyun, C. (1995), "Prediction of thermal stress of high-strength concrete and massive concrete", Ph.D Thesis, The University of Tokyo, Tokyo, Japan.
- Lura, P., Jensen, O.M. and Breugel, K.V. (2003), "Autogenous shrinkage in high-performance cement paste:

- An evaluation of basic mechanisms”, *Cement Concrete Res.*, **33**(2), 223-232.
- Maekawa, K., Ishida, T. and Kishi, T. (2009), *Multi-scale Modeling of Structural Concrete*, London and New York, Taylor & Francis.
- Maruyama, I. , Suzuki, M. and Sato, R. (2005), “Prediction of temperature in ultra high-strength concrete based on temperature dependent hydration model”, *ACI SP-228, Proceeding of 7th International Symp on High Performance Concrete (Edited by Henry G. Russell)* , Washington, D.C., pp.1175-1186.
- Papadakis, V.G. (1999), “Experimental investigation and theoretical modeling of silica fume activity in concrete”, *Cement Concrete Res.*, **29**(1), 79-86.
- Papadakis, V.G. (2000), “Effect of supplementary cementing materials on concrete resistance against carbonation and chloride”, *Cement Concrete Res.*, **30**(2), 291-299.
- Park, K.B., Jee, N.Y., Yoon, I.S. and Lee, H.S. (2008), “Prediction of temperature distribution in high-strength concrete using hydration model”, *ACI. Mater. J.*, **105**(2), 180-186.
- Saeki, T. and Monteiro, P.J.M. (2005), “A model to predict the amount of calcium hydroxide in concrete containing mineral admixture”, *Cement Concrete Res.*, **35**(10), 1914-1921.
- Song, H.W. and Kwon, S.J. (2009), “Evaluation of chloride penetration in high performance concrete using neural network algorithm and micro pore structure”, *Cement Concrete Res.*, **39** (9), 814-824.
- Tang, C.W. (2010), “Hydration properties of cement pastes containing high-volume mineral admixtures”, *Comput. Concr.*, **7**(1), 17-38.
- Tian, Y., Jin, X. and Jin, N. (2013), “Thermal cracking analysis of concrete with cement hydration model and equivalent age method”, *Comput. Concr.*, **11**(4), 271-289
- Tomosawa, F. (1997), “Development of a kinetic model for hydration of cement”, *Proceedings of tenth international congress chemistry of cement (Edited by S. Chandra)*, Gothenburg.
- Wang, C. and Dilger, W.H. (1994), “Prediction of temperature distribution in hardening concrete”, *Proceeding of Thermal Cracking in Concrete at Early Ages (Edited by R.Spingenschmid)*, London.
- Wang, X.Y. and Lee, H.S. (2010), “Modeling the hydration of concrete incorporating fly ash or slag”, *Cement Concrete Res.*, **40**(7), 984-996.